Der **Dannie-Heinemann-Preis 2015** wurde Andrea Cavalleri, Hamburg, für seine zeitaufgelösten Messungen an lichtinduzierten Phasenübergängen in hochkorrelierten Elektronensystemen verliehen.

Andrea Cavalleri
Controlling Complex Solids with Light

Andrea Cavalleri, Professor am Max-Planck Institut für Struktur und Dynamik der Materie in Hamburg, Träger des Dannie-Heinemann-Preises 2015

Materials with complex electronic properties are one of the backbones of modern technology. Doped semiconductors with high electron mobility, magnetic multilayers with large (giant) magnetoresistance and superconducting alloys permeate most of our daily lives. Applications range from cellular phones, to memory devices, or MRI diagnostic machines for health. In all of these, collective quantum phenomena play a crucial role.

Recent advances in this area have been seen in "quantum" solids with "unconventional" behavior. These terms are often used loosely to indicate materials in which the following features are realized:

1) Important functionalities are observed at "high temperatures". Temperatures are considered "high", for example in the case of superconductivity in the cuprates when these are close to room temperature. However, more rigorous definitions compare the temperature scale to the kinetic energy of electrons (electronic bandwidths) or to Fermi temperatures T_f. Hence, highly unconventional and "high-temperature" phenomena are sometimes those found at low absolute temperatures in, for example, molecular solids or heavy fermion materials.
2) The macroscopic properties of such unconventional quantum materials are highly sensitive to external perturbations. Due to the underlying nonlinearities and the interaction between many microscopic degrees of freedom, functional properties emerge amongst many possible, competing states. The response to external stimulation can also be very large, that is, it is not uncommon to see changes in the conductivity of a compound of many orders of magnitude upon application of, say, a magnetic field. These are highly

10.1515/JBG-2015-0013

attractive features of these materials, which are seen as an important new horizon for device applications.

3) At a microscopic level, interactions between charge carrying excitations and all degrees of freedom are uncommonly strong, introducing a dominant energy scale. In such "strongly correlated electron" systems, familiar concepts of band theory and classical magnetism fail to describe even basic phenomena.

These complex solids have received renewed attention in a quest to understand the physics of high-temperature superconductivity in doped cuprates. However, along the way, a wealth of new phenomena have been discovered, including unconventional electronic and magnetic phase transitions[1], colossal negative magnetoresistance[2], and novel effects at interfaces[3]. Such richness arises from the peculiar physics of partially filled electronic shells of transition metals, which dominate transport and magnetic properties. On the one hand, electrons in these orbitals tend to localize on the transition metal site due to their enormous mutual repulsion, making the system insulating. Yet, the same electrons are also on the verge of de-localizing, as they tend to hybridize with extended 2p orbitals from their oxygen neighbors and spread over many lattice sites to minimize their kinetic energy. When this happens, a metal is formed and magnetic arrangements tend to change as well.

Nowhere is this competition more striking than in the abrupt electronic and magnetic transitions observed with changes in the density of conducting electrons, as controlled by chemical doping. Similarly, because of the importance of next-neighbor orbital overlap, small distortions in lattice structure can equally cause colossal changes in transport and magnetic properties.

It is then also easy to see how excitation with light, which rearranges electrons amongst different orbitals, can trigger important transformations in the macroscopic structural, electronic and magnetic properties of a complex solid. Due to the cooperative nature of these rearrangements, it is not uncommon to observe switching of the whole solid for excitation densities of as little as one absorbed photon every 1000 unit cells.

Much of the work recognized by this award involves a new and potentially far more direct form of optical control. Instead of visible and near visible excitation with optical lasers, we use THz frequency transients, that is, at frequencies nearly one hundred times lower than the optical range, to stimulate solids.

---

1 M. Imada, A. Fujimori, Y. Tokura Rev of Mod Phys. 70, 1039 (1998)

2 M.B. Salamon, M. Jaime Rev. Mod. Phys. 73, 583 (2001).

3 A. Ohtomo and H.Y. Hwang Nature 427, 423 (2004).

1 Nonlinear Phononics

Terahertz (THz) frequency optical fields at strengths in excess of 100 kV/cm can be used to resonantly excite collective modes in solids, provided that these modes are at long wavelengths (q ~ 0) and infrared-active, that is, changes in their coordinate Q involve a change in dipole moment. Lattice vibrations can selectively be driven to amplitudes as high as several percent of unit cell distances. A situation in which all modes are at low temperatures, whereas one is populated coherently to such large amplitude, is a new and highly unusual. Crucially, dynamical states are created that may have radically different *average* properties than the same materials at equilibrium.

The linear response of a crystal lattice to a light field made resonant with an infrared-active phonon mode is described by the potential energy term $H_{lin} = \frac{1}{2}\omega_{IR}^2 Q_{IR}^2$. In this expression, Q_{IR} is the normal coordinate of the mode and ω_{IR} its frequency. When resonantly driven by a pulsed field of the type $f(t) = F(t)sin(\omega_{IR}t)$, for which $F(t)$ is a Gaussian envelope function, the dynamics can be described by the equation of motion of a damped harmonic oscillator

$$\ddot{Q}_{IR} + 2\gamma_{IR}\dot{Q}_{IR} + \omega_{IR}^2 Q_{IR} = f(t), \tag{1}$$

where γ_{IR} is damping constant of the mode. Following the excitation, the atoms oscillate about their equilibrium positions along the normal coordinate of the mode and relax over a timescale determined by the duration of the envelope function or by the decay time $1/\gamma_{IR}$, whichever is longer.

By increasing the strength of the driving electric field, anharmonic coupling to other modes with generic coordinate Q_R becomes important. In the limit of cubic coupling, the lattice Hamiltonian describing the nonlinear interaction reads

$$H_{NL} = \frac{1}{2}\omega_R^2 Q_R^2 - a_{12} Q_{IR} Q_R^2 - a_{21} Q_{IR}^2 Q_R \tag{2}$$

where a_{ij} are the anharmonic coupling constants. Equation (2) is simplified if we consider only centrosymmetric crystals, for which infrared-active phonon modes are of odd parity while Raman-active modes are even.

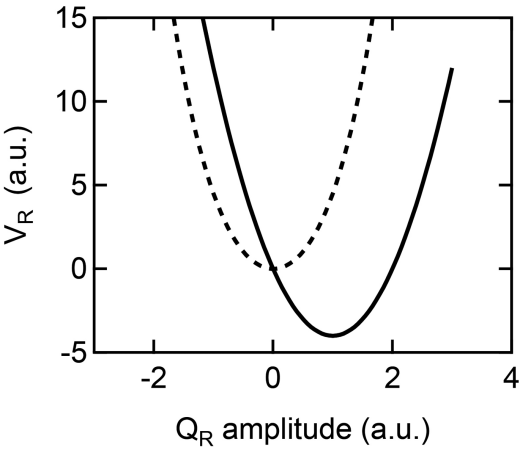

Fig. 1: Parabolic energy potential V_R of a Raman-active phonon mode (dashed curve). Within cubic coupling, this energy potential shifts towards a new position (solid curve) for a finite static displacement of a coupled infrared-active mode Q_{IR}.

For these symmetry reasons, the first coupling term $a_{12}Q_{IR}Q_R^2$ is always zero and the second term $a_{21}Q_{IR}^2Q_R$ is nonzero only if Q_R is a Raman mode. For a finite static displacement Q_{IR}^* of the infrared-active mode, this nonlinear phonon interaction induces a shift of the Raman modes energy potential, as depicted in Figure 1. These physics were analyzed theoretically in the 1970ies, casted in the framework of Ionic Raman scattering[4, 5, 6].

For pulsed excitation of the infrared-active mode Q_{IR}, the coupled dynamics are described by the two equations of motion, which take the form

$$\ddot{Q}_{IR} + 2\gamma_{IR}\dot{Q}_{IR} + \omega_{IR}^2 Q_{IR} = 2a_{21}Q_{IR}Q_R + f(t) \tag{3}$$

$$\ddot{Q}_R + 2\gamma_R\dot{Q}_R + \omega_R^2 Q_R = a_{21}Q_{IR}^2 \tag{4}$$

Key to the dynamics of the anharmonically coupled Raman mode Q_R is the driving force $a_{21}Q_{IR}^2$ with its direction being independent of the sign of Q_{IR}.

4 Wallis R.F.; Maradudin A. A. Ionic Raman effect II: The first-order ionic Raman effect. Phys. Rev. B 1971, 3, 2063.

5 Martin T.P. and Genzel L. Ionic Raman scattering and ionic frequency mixing. Phys. Status Solidi B 1974, 61, 493.

6 Mills D.L. Ionic contribution to the Raman tensor of insulators. Phys. Rev. B 1987, 35, 9278.

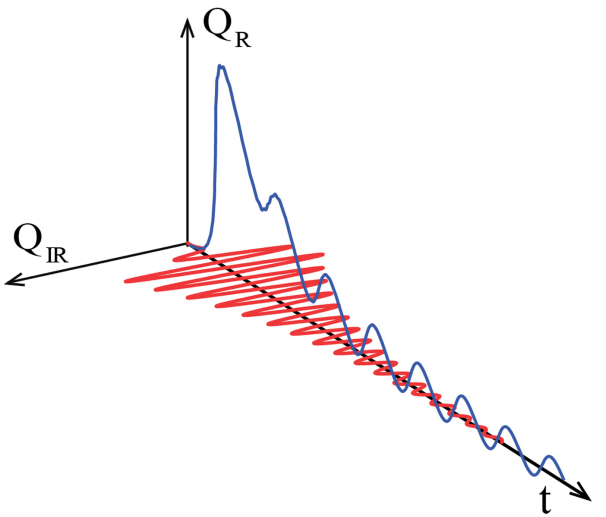

Fig. 2: The dynamical response of the two modes within cubic coupling. The infrared-active mode Q_{IR} (red) oscillates coherently about the equilibrium position, while Q_R (blue) undergoes a directional displacement, which scales with Q_{IR}^2 and survives as long as the Q_{IR} amplitude is finite. If the optical excitation is short compared to the Raman phonon period, coherent oscillations along Q_R take place, which decay with the dephasing time of the Raman mode.

Hence, the atoms of the crystal lattice not only oscillate along the infrared coordinate Q_{IR}, but are simultaneously displaced along the Raman coordinate Q_R (see Figure 2). This effect is the equivalent of rectification in nonlinear optics. Furthermore, if the optical excitation is short compared to the period of the Raman mode, Q_R oscillates coherently around the quasi-static displacement amplitude.

These two effects, a displacement and oscillations, are also characteristic of the well-known coherent response of crystal lattices to pulsed excitation in the near-IR or visible[7, 8, 9]. However, in that case the lattice displacement and oscillations are driven by electron-phonon coupling and not, as it is the case for nonlinear phononics, by lattice anharmonicities. Note also that the excitation through nonlinear phononics is more selective and dissipation far reduced. Furthermore, the lattice displacement consists as long as the infrared mode oscillates

7 Dhar L.; Rogers J.; Nelson K.A. Time-resolved vibrational spectroscopy in the impulsive limit. Chem. Rev. 1994, 94, 157.

8 Merlin R. Generating coherent THz phonons with light pulses. Solid State Commun. 1997, 102, 207.

9 Stevens T.E.; Kuhl J.;Merlin R. Coherent phonon generation and the two stimulated Raman tensors. Phys. Rev. B 2002, 65, 144304.

and can thus potentially be controlled by using pulse trains or varying the duration of the excitation pulses.

2 Driving Phase Transitions by Phononoics

2.1 Nonlinear lattice dynamics

The first experimental observation of nonlinear phononics was achieved in the magnetoresistive perovskite $La_{0.7}Sr_{0.3}MnO_3$, a double-exchange ferromagnet with low electrical conductivity below T_c ~350 K. The infrared-active phonon mode, which was resonantly excited by mid-infrared pump pulses to large amplitudes, comprises Mn-O stretching motions at a frequency of ~18 THz (75 meV) and is of E_u symmetry[10].

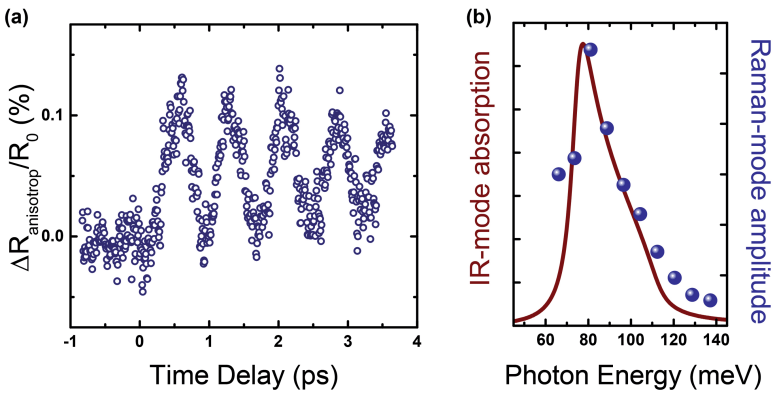

Fig. 3: (a) Time-resolved anisotropic reflectivity changes in $La_{0.7}Sr_{0.3}MnO_3$ induced by the resonant excitation of the infrared-active E_u-symmetry Mn-O stretching mode at 14.3 μm wavelength (87 meV photon energy). The excitation fluence is 2 mJ/cm^2. (b) Amplitude of the coherent E_g-symmetry Raman phonon as function of the pump photon energy. Figures adapted from Ref. 11.

Figure 3(a) displays the time dependent anisotropic optical reflectivity changes that follow the excitation of this mode, measured in a pump-probe setup utilizing mid-infrared (14.3 μm wavelength) pump – near-infrared (800 nm wavelength)

10 Okimoto Y.; Katsufuji T.; Ishikawa T.; Arima T.; Tomioka Y.; Tokura Y. Variation of electronic structure in $La_{1-x}Sr_xMnO_3$ (0<x<0.3) as investigated by optical conductivity spectra. Phys. Rev. B 1997, 55, 4206.

probe pulses[11]. Strikingly, the ultrafast optical response exhibits reflectivity oscillations at 1.2 THz, which – because of their frequency and their the anisotropic response – can be attributed to a Raman mode of E_g symmetry that involves the rotation of oxygen octahedra around the Mn cations[12, 13].

2.2 Driving insulator-metal transitions

The observed conversion of the resonantly driven Mn-O stretching oscillations in $La_{0.7}Sr_{0.3}MnO_3$ into the rotation of the MnO_6 oxygen octahedra, which are strongly coupled to the collective electronic and magnetic properties, opens intriguing possibilities for the phase control of manganites. Rotations of the MnO_6 octahedra modify the Mn-O-Mn bond angles, which changes the degree of spatial overlap of the orbital wavefunctions along these bonds and controls the sign of the exchange interactions[14, 15]. In particular, the probability of *3d* electrons for hopping between adjacent Mn sites is maximum for a bond angle of 180° (cubic lattice) and decreases with decreasing angle, resulting in maximum electron bandwidth for straight bonds. The magnetic and structural properties of manganites can be understood in more detail by considering the Goodenough-Kanamori (GK) rules for semicovalent bonds[16], which explain the exchange interactions between neighboring manganese cations (Mn^{3+} or Mn^{4+}) connected by an oxygen anion (O^{2-}). For doped manganites, both ferromagnetic metallic or antiferromagnetic insulating behavior is possible. For asymmetric Mn^{3+}– O^{2-}– Mn^{4+} bonds, hopping occurs and the magnetic coupling is ferromagnetic as long as the bond is "straight". A "bent" bond, with an angle $<180^O$ corresponds to an insulating, antiferromagnetic phase.

Due to this interplay, the octahedral manganite $Pr_{0.7}Ca_{0.3}MnO_3$ is an insulator because of its strongly distorted perovskite structure. However, these properties are unstable against various forms of external perturbation, including electric or

---

11 Först M.; Manzoni C.; Kaiser S.; Tomioka Y.; Tokura Y.; Merlin R.; Cavalleri A. Nonlinear phononics as an ultrafast route to lattice control. Nature Physics 2011, 7, 854.

12 Abrashev M.V.; Litvinchuk A.P.; Iliev M.N.; Meng R.L.; Popov V.N.; Ivanov V.G.; Chalakov R.A.; Thomsen C. Comparative study of optical phonons in the rhombohedrally distorted perovskites $LaAlO_3$ and $LaMnO_3$. Phys. Rev. B 1999, 59, 4146.

13 Granado E.; Moreno N.O.; Garcia V; Sanjurjo J.A.; Rettori C.; Torriani V.; Oseroff S.B.; Neumeier J.J.; McClellan K.J.; Cheong S.-W.; Tokura Y. Phonon Raman scattering in $R_{1-x}A_xMnO_{3+\delta}$ (R=La, Pr; A=Ca, Sr). Phys. Rev. B 1998, 58, 11435.

14 Anderson, P.W.; Hasegawa, H. Considerations on double exchange. Phys. Rev. 1955, 100, 675.

15 Imada, M.;Fujimori, A.; Tokura, Y. Metal-insulator transitions. Rev. Mod. Phys. 1998, 70, 1039.

16 Goodenough J.B. Theory of the Role of Covalence in the Perovskite-Type Manganites [La, M(II)]MnO_3. Phys. Rev. 1955, 100, 564.

magnetic fields and light[17, 18, 19, 20, 21]. Importantly, a metallic phase can also be induced by application of static pressure[22], which qualitatively can be understood as "straightening" of the bonds.

The dynamical lattice control of the electronic phase state of a manganite was first reported by Rini et al.[23], who measured the electric transport properties in a $Pr_{0.7}Ca_{0.3}MnO_3$ single crystal after resonant excitation of the Mn-O stretching mode.

Excitation of the sample with ~1mJ/cm^2 femtosecond pulses at ~17 μm wavelength induced transient changes in electric transport, as shown in Figure 4(a). The transition from the insulating ground state into the metastable metallic state is evident from the five-order-of-magnitude increase in electrical conductivity within the first 5 nanoseconds.

Importantly, as the nonlinear phonon response in $La_{0.7}Sr_{0.3}MnO_3$ discussed above, the strength of the insulator-metal transition in $Pr_{0.7}Ca_{0.3}MnO_3$ clearly peaks at the resonance of the Mn-O stretching mode (see Figure 4(b)). Hence, the light-driven phase transition is not related to the injection of charge carriers and can be uniquely attributed to large-amplitude crystal lattice distortions.

---

17 Tomioka Y; Asamitsu A.; Kuwahara H.; Moritomo Y. Magnetic-field-induced metal-insulator phenomena in $Pr_{1-x}Ca_xMnO3$ with controlled charge-ordering instability. Phys. Rev. B 1996, 53, 1689.

18 Asamitsu A.; Tomioka Y.; Kuwahara H.; Tokura Y. Current switching of resistive states in magnetoresistive manganites. Nature 1997, 388, 50.

19 Kiriukhin V.; Casa D.; Hill J.P.; Keimer B.; Vigliante A.; Tomioka Y.; Tokura Y. An X-ray-induced insulator–metal transition in a magnetoresistive manganite. Nature 1997, 386, 813.

20 Miyano K.; Tanaka T.; Tomioka Y.; Tokura Y. Photoinduced Insulator-to-Metal Transition in a Perovskite Manganite. Phys. Rev. Lett. 1997, 78, 4257.

21 Fiebig M.; Miyano K.; Tomioka Y.; Tokura Y. Visualization of the Local Insulator-Metal Transition in $Pr_{0.7}Ca_{0.3}MnO_3$. Science 1998, 280, 1925.

22 Hwang H.Y.; Palstra T.T.M.; Cheong S.-W.; Batlogg B. Pressure effects on the magnetoresistance in doped manganese perovskites. Phys. Rev. B 1995, 52, 15046.

23 Rini M.; Tobey R.; Dean N.; Itatani J.; Tomiaka Y.; Tokura Y.; Schoenlein R.W.; Cavalleri A. Control of the electronic phase of a manganite by mode-selective vibrational excitation, Nature 2007, 449, 72.

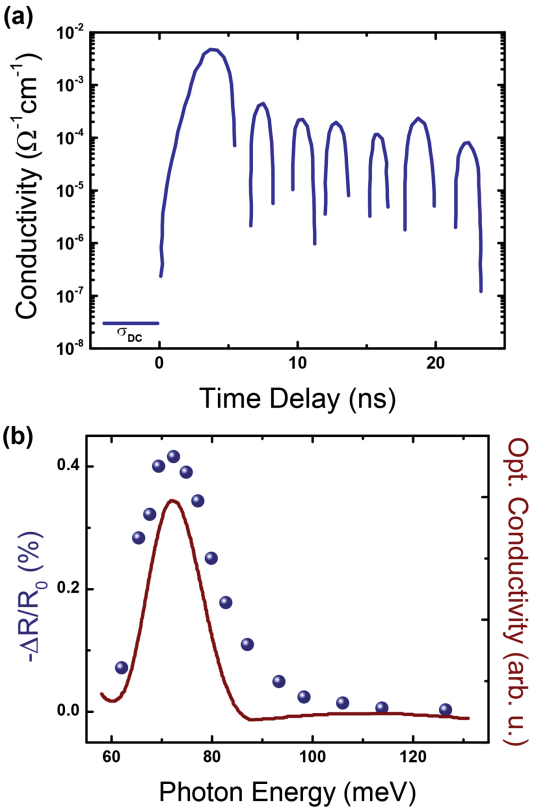

Fig. 4: (a) Time-dependent electric conductivity of a $Pr_{0.7}Ca_{0.3}MnO_3$ single crystal, measured by direct current transport with a fast oscilloscope, following resonant excitation of the Mn-O stretching vibration in the mid-infrared. The DC conductivity is drastically increased as result of the vibrationally driven insulator-to-metal transition. The time resolution of this experiment was 4 ns, and the ringing at later time delays results from the fast conductivity changes and the resulting lack of impedance matching with the oscilloscope. (b) Dependence of the strength of the insulator-metal transition as function of the mid-infrared photon energy, compared with the $Pr_{0.7}Ca_{0.3}MnO_3$ optical conductivity (that is convolved with the spectral width of the excitation pulses). Figure adapted from Ref. 23.

This conclusion was recently substantiated by a microscopic theory, which predicts the dynamical path taken by the crystal lattice and its affect on the electronic material properties. Subedi et al.[24] used density functional theory to compute the

24 Subedi, A.; Cavalleri A.; Georges A. Theory of nonlinear phononics for coherent light control of solids. Phys. Rev. B 2014, 89, 220301.

coupling strength of the resonantly driven Mn-O stretching mode to other phonon modes in the parent compound $PrMnO_3$. The energy potential of the strongly coupled A_g symmetry Raman mode for various amplitudes Q_{IR} of the infrared-active B_{1u} symmetry Mn-O stretching mode is shown in Fig. 6(a).

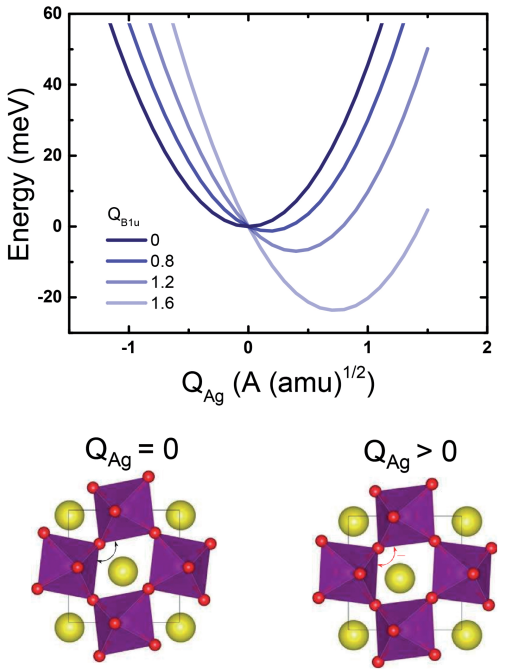

Fig. 5: Calculated energy potential of the A_g in-plane rotational Raman mode in $PrMnO_3$ for different static displacements of the infrared-active B_{1u} mode. The bottom panel sketches atomic positions of the orthorhombically distorted perovskite at equilibrium (left) and for finite positive amplitude Q_{Ag} of the in-plane rotational Raman mode (right). Figure adapted from Ref. 24.

Finite displacement of the crystal lattice along the B_{1u} coordinate shifts the parabolic potential of the A_g mode to a new minimum position. As expected for the cubic $Q^2_{B1u}Q_{Ag}$ phonon coupling, this displacement of the Raman mode from the equilibrium increases quadratically with the amplitude of the infrared mode. As shown in lower panel of Fig. 5, the atomic motions associated with the positive amplitude reduce the rotation of the MnO_6 octahedra in the *ab*-plane, hence bringing the crystal structure closer to the cubic perovskite and straightening the Mn-O-Mn bonds.

According to nonlinear phononics, the excitation of the B_{1u} mode by an intense mid-infrared pulse will transiently displace the crystal lattice along these

coordinates. In order to show that these motions are responsible for driving the insulator-to-metal-transitions, the electronic density of states of the manganese *3d* orbitals in this compound were also calculated by dynamical mean field theory.

3 Enhancing Superconductivity by Nonlinear Phononics

We have introduced above how nonlinear lattice dynamics in the doped manganites can melt drive an insulator metal transition. In cuprates, which show high-temperature superconductivity, the same nonlinear phonon excitation has been used to remove competing charge order and promote superconductivity up to the room temperature scale.

3.1 Light-induced superconductivity in single layer La cuprates

La_2CuO_4 is an antiferromagnetic Mott insulator. As holes are doped into the CuO_2 planes by chemical substitution to $La_{2-x}(Ba/Sr)_xCuO_4$, an unconventional metallic phase appears that transforms into a superconductor for $x > 0.05$ and reaches the highest critical temperatures T_C near optimal doping of $x = 0.16$. The $x = 1/8$ compound deserves special attention due to the appearance of a periodic one-dimensional modulation of charges and spins[25, 26] and a concomitant sharp reduction in T_C[27, 28]. In the Ba-doped system, these "stripes" become static, enhanced by periodic buckling of the CuO_2 planes[29, 30, 31].

---

25 Zaanen J.; Gunnarson O. Charged magnetic domain lines and the magnetism of high-Tc oxides Phys. Rev. B 1989, 40, 7391.

26 Tranquada J.; Sternlieb B.J.; Axe J.D.; Nakamura Y.; Uchida S. Evidence for stripe correlations of spins and holes in copper oxide superconductors. Nature 1995, 375, 561.

27 Moodenbaugh A.R.; Xu Y.; Suenaga M.; Folkerts T.J.; Shelton R.N. Superconducting properties of $La_{2-x}Ba_xCuO_4$. Phys. Rev. B 1988, 38, 4596.

28 Hücker, M.; von Zimmermann M.; Gu G.; Xu Z.; Wen J.; Xu G.; Kang H.; Zheludev A.; Tranquada J. Stripe order in superconducting $La_{2-x}Ba_xCuO_4$ (0. 095<x<0.155). Phys. Rev. B 2011, 83, 104506.

29 Suzuki, T.; Fujita T. Low-temperature crystalline structure of $(La_{1-x}Ba_x)_2CuO_{4-\delta}$. Physica C 1989, 159, 111.

30 Crawford M.K.; Harlow R.L.; McCarron E.M.; Farneth W.E.; Axe J.D.; Chou H.; Huang Q. Lattice instabilities and the effect of copper-oxygen-sheet distortions on superconductivity in doped La_2CuO_4. Phys. Rev. B 1991, 44, 7749.

31 Fujita M.; Goka H.;Yamada K.; Matsuda M. Competition between charge- and spin-density-wave order and superconductivity in $La_{1.875}Ba_{0.125-x}Sr_xCuO_4$. Phys. Rev. Lett. 2002, 88, 167008.

Figure 6a) shows a schematic structure of this compound depicting CuO_2 layers stacked along the crystallographic *c* axis. The critical temperature of $LESCO_x$ is strongly reduced for all doping values below and completely suppressed at x=1/8, as illustrated in the phase diagram (Fig. 10b))[32, 33].

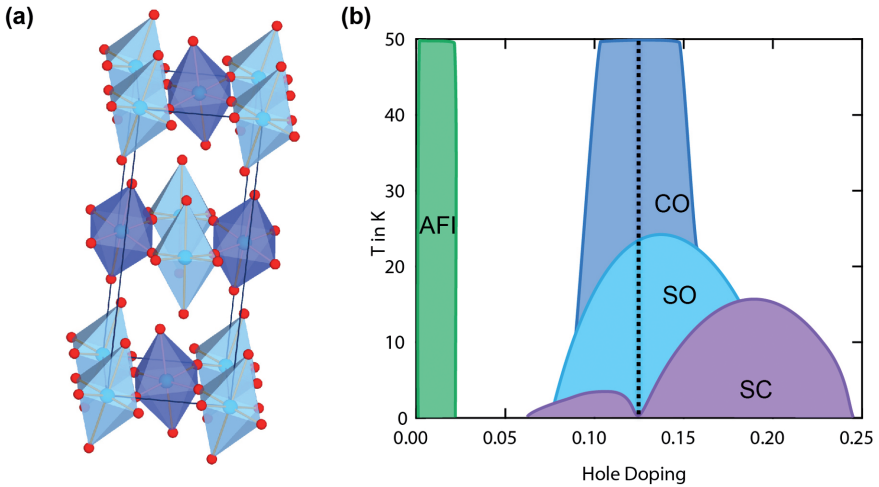

Fig. 6: (a) Schematic crystal structure and (b) phase diagram for $La_{1.8-x}Eu_{0.2}Sr_xCuO_4$ ($LESCO_x$). This compound is an antiferromagnetic insulator at zero doping. A low-temperature structural distortion, associated with buckling of the Cu-O planes, quenches superconductivity at all doping levels below 1/8 (vertical dashed line). At this doping, a one-dimensional modulation of charges (CO) and spins (SO), the stripe state, emerges in the planes. At doping levels above 1/8, the compound is superconducting.

Understanding the relationship between the superconducting state, stripe order, and the LTT distortion is one of the grand goals in high-T_C superconductivity. It has long been believed that stripes are pinned by the LTT distortion and compete with superconductivity to result in a non-superconducting state. Virtually all studies have explored this interplay by changing static doping or by adiabatically tuning an external parameter. For example, the application of pressure has been

32 Klauss H.-H.; Wagener W.; Hillberg M.; Kopmann W.; Walf H.; Litterst F.J.; Hücker M.; Büchner B. From antiferromagnetic order to static magnetic stripes: The phase diagram of $(La, Eu)_{2-x}Sr_xCuO_4$. Phys. Rev. Lett. 2000, 85, 4590.

33 Suryadijaya, Sasakawa T.; Takagi H. Oxygen isotope effect on charge/spin stripes in $La_{1.8-x}Eu_{0.2}Sr_xCuO_4$. Physica C 2005, 426, 402.

shown to restore superconductivity by perturbing the equilibrium crystallographic structure[34, 35].

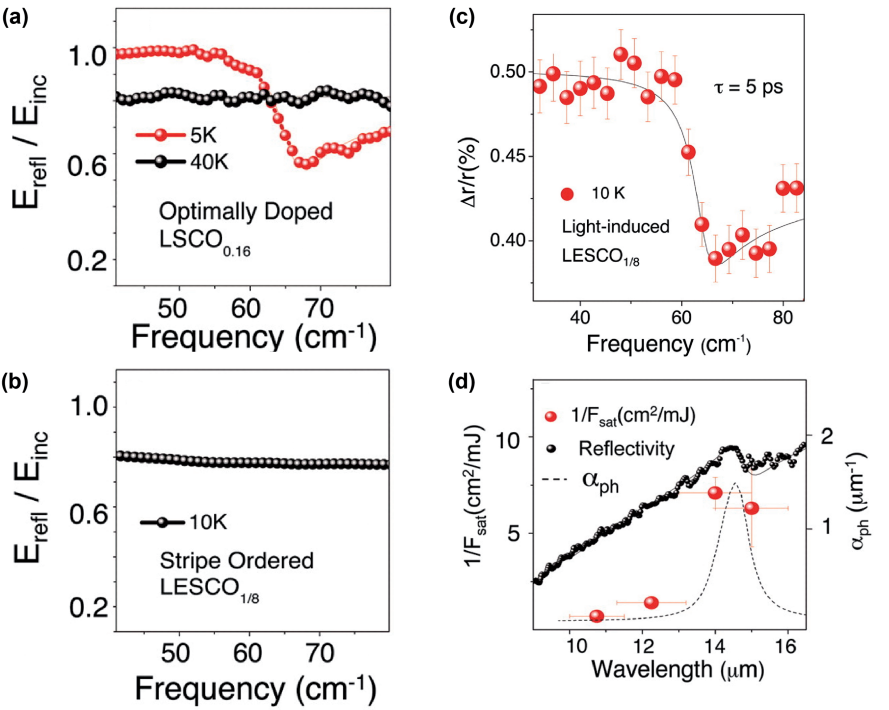

Fig. 7: (a) Static c-axis electric-field reflectance of $La_{1.84}Sr_{0.16}CuO_4$ ($LSCO_{0.16}$). In the superconducting state at 5 K < T_C = 35 K, the appearance of a Josephson plasma edge reflects the coherent inter-layer transport. Above T_C, incoherent ohmic transport is reflected in a featureless conductivity. (b) Static c-axis reflectance of $La_{1.675}Eu_{0.2}Sr_{0.125}CuO_4$ ($LESCO_{1/8}$) at 10 K, showing the optical properties of a non-superconducting compound. (c) Phonon-excitation induced *c*-axis reflectance of ($LESCO_{1/8}$) at 10 K, normalized to the static reflectance, showing a Josephson plasma edge that evidences the photo-induced superconducting-like state. (d) Inverse threshold (photo-susceptibility) as a function of pump wavelength (red dots) compared to the static mid-infrared $LESCO_{1/8}$ reflectivity in the *ab* plane (black dots). The extinction coefficient α (dashed curve) is extracted by means of a Drude-Lorentz fit. Figures taken from Ref. 36.

---

34 Takeshita N.; Sasagawa T.; Sugioka T.; Tokura Y.; Takagi H. Gigantic anisotropic uniaxial pressure effect on superconductivity within the CuO_2 plane of $La_{1.64}Eu_{0.2}Sr_{0.16}CuO_4$: Strain control of stripe criticality. Journ. Phys. Soc. Jpn. 2004, 73, 1123.

35 Hücker M.; von Zimmermann M.; Debessai M.; Schilling J.S.; Tranquada J.M.; Gu G.D. Spontaneous symmetry breaking by charge stripes in the high pressure phase of superconducting $La_{1.875}Ba_{0.125}CuO_4$. Phys. Rev. Lett. 2010, 104, 057004.

Fausti et al. dynamically perturbed the lattice of non-superconducting $LESCO_{1/8}$ by selectively driving an infrared-active lattice vibration with mid-infrared femtosecond pulses[36]. A single-crystal sample, held at a base temperature of 10 K, was excited at 16 μm wavelength (70 meV photon energy), resonant with an in-plane Cu-O stretching mode comparable to that driven in the manganites. Above a threshold fluence of 0.1 mJ/cm^2, the 800-nm reflectivity, which is at least indirectly related to the appearance of superconductivity[37, 38], shows a prompt and long-lived increase following this excitation.

This vibrationally driven state of $LESCO_{1/8}$ was then shown to be superconducting by using time-resolved THz spectroscopy. At equilibrium, superconductivity in the layered cuprates is reflected in the appearance of a Josephson Plasma Resonance (JPR) in the *c*-axis THz optical properties. This resonance is a general feature observed in layered cuprate superconductors[39], well understood by considering coupling between stacks of quasi-two-dimensional superconducting CuO_2 layers to explain the three-dimensional superconducting state[40, 41, 42]. Figure 7(a) reports the static *c*-axis electric-field reflectance of optimally doped $La_{1.84}Sr_{0.16}CuO_4$ below and above the critical temperature T_C = 35 K. A plasma edge near 60 cm^{-1} wave numbers emerges in the reflectance of the superconducting state. Above the critical temperature, where interlayer transport is incoherent, the THz spectral response of $La_{1.84}Sr_{0.16}CuO_4$ becomes flat (Fig. 7(a), black data points). The equilibrium THz electric-field reflectance of non-superconducting $LESCO_{1/8}$ shown in Figure 7(b) is also featureless.

Figure 7(c) reports the THz-reflectance in $LESCO_{1/8}$ measured five picoseconds after the 16-μm mid-infrared excitation of the in-plane Cu-O stretch mode.

---

36 Fausti D.; Tobey R.I.; Dean N.; Kaiser S.; Dienst A.; Hoffmann M.C.; Pyon S.; Takayama T.; Takagi H.; Cavalleri A. Light induced Superconductivity in a Stripe-ordered Cuprate. Science 2011, 331, 6014.

37 Segre G.P.; Gedik N.; Orenstein J.; Bonn D.A.; Liang R.; Hardy W.N. Photoinduced changes of reflectivity in single crystals of $YBa_2Cu_3O_{6.5}$ (Ortho II). Phys. Rev. Lett. 2002, 88, 137001.

38 Giannetti C.; Coslovich G.; Cilento F.; Ferrini G.; Eisaki H.; Kaneko N.; Greven M.; Parmigiani F. Discontinuity of the ultrafast electronic response of underdoped superconducting $Bi_2Sr_2CaCu_2O_{8+\delta}$ strongly excited by ultrashort light pulses. Phys. Rev. B 2009, 79, 224502.

39 Tamakasu K.; Nakamura Y.; Uchida S. Charge dynamics across the CuO_2 planes in $La_{2-x}Sr_xCuO_4$. Phys. Rev. Lett. 1992, 69, 1455.

40 Kleiner R.; Steinmeyer F.; Kunkel G.; Müller P.; Intrinsic Josephson effects in $Bi_2Sr_2CaCu_2O_8$ single crystals. Phys. Rev. Lett. 1992, 68, 2394.

41 Basov D.N.; Timusk T.; Dabrowski B.; Jorgensen J.D. c-axis response of $YBa_2Cu_4O_8$: A pseudogap and possibility of Josephson coupling of CuO2 planes Phys. Rev. B 1994, 50, 3511.

42 Tajima S.; Noda T.; Eisaki H.; Uchida S. c-Axis optical response in the static stripe ordered phase of the cuprates. Phys. Rev. Lett. 2001, 86, 500.

Clearly, a plasma edge was observed at a frequency comparable to that measured in $LSCO_{0.16}$, evidencing the emergence of photo-induced superconducting-like transport along the *c* axis in $LESCO_{1/8}$. Figure 7(d) plots the pump-wavelength dependence of the inverse fluence threshold for the photo-induced superconductivity in $LESCO_{1/8}$, used as a measure of photo-susceptibility. This data was compared to the wavelength dependent extinction coefficient α near the phonon resonance (dashed line). The observed clear resonance of the photo-susceptibility at the Cu-O stretching mode frequency proved that direct coupling of the light electric field to the crystal structure triggers formation of the superconducting phase.

The light-induced Josephson coupling of the CuO_2 planes itself was hypothesized to be the consequence of an instantaneous stripe order melting, mediated by the direct distortion of the lattice through the mid-infrared excitation. The fast time scale of this recoupling was taken as indirect support for the picture of a two-dimensional "pair-density wave" coherent state[43], in which the charge stripe order suppresses superconductivity only along the *c* axis. Indeed, stripes are compatible with in-plane Cooper pairing in a scenario, where two-dimensional superconducting CuO_2 planes are decoupled due to the periodic charge modulation that prevent interlayer Josephson tunneling[44].

In a second experiment, the fate of the charge stripe order and of the LTT distortion in the transient 3D coherent superconductor, following the mid-IR excitation pulse, was probed in the strongly related stripe-ordered $La_{1.875}Ba_{0.125}CuO_4$. Först et al. used femtosecond resonant soft x-ray diffraction at the LCLS free electron laser to provide insight into the microscopic physics underlying this light-induced state[45]. Both static stripe order and the LTT distortion were measured through resonant diffraction near the oxygen K-edge. Here, static charge stripes can be observed at the $\boldsymbol{Q}$ = (0.24 0 0.5) wave vector[46, 47],

43 Li Q.; Hücker M.; Gu G.D.; Tsvelik A.M.; Tranquada J. Two-dimensional superconducting fluctuations in stripe-ordered $La_{1.875}Ba_{0.125}CuO_4$. Phys. Rev. Lett. 2007, 99, 067001.

44 Berg E.; Fradkin E.; Kim E.-A.; Kivelson S.A.; Oganesyan V.; Tranquada J.M.; Zhang S.C. Dynamical layer decoupling in a stripe-ordered high-T_C superconductor. Phys. Rev. Lett. 2007, 99, 127003.

45 Först M. et al. Melting of charge stripes in vibrationally driven $La_{1.875}Ba_{0.125}CuO_4$: Assessing the respective roles of electronic and lattice order in frustrated superconductors. Phys. Rev. Lett. 2014, 112, 157002.

46 Abbamonte P.; Rusydi A.; Smadici S.; Gu G.D; Sawatzky G.A.; Feng and D.L Spatially modulated 'Mottness' in $La_{2-x}Ba_xCuO_4$. Nature Physics 2005, 1, 155.

47 Wilkins S.B.; Dean M.P.M.; Fink J.; Hücker M.; Geck J.; Soltwisch V.; Schierle E.; Weschke E.; Gu G.; Uchida S.; Ichikawa N.; Tranquada J.M., Hill J.P. Comparison of stripe modulations in $La_{1.875}Ba_{0.125}CuO_4$ and $La_{1.48}Nd_{0.4}Sr_{0.12}CuO_4$. Phys. Rev. B 2011, 84, 195101.

[48], whilst the LTT distortion can be directly measured through the (001) diffraction peak that is structurally forbidden in the high-temperature phases[49].

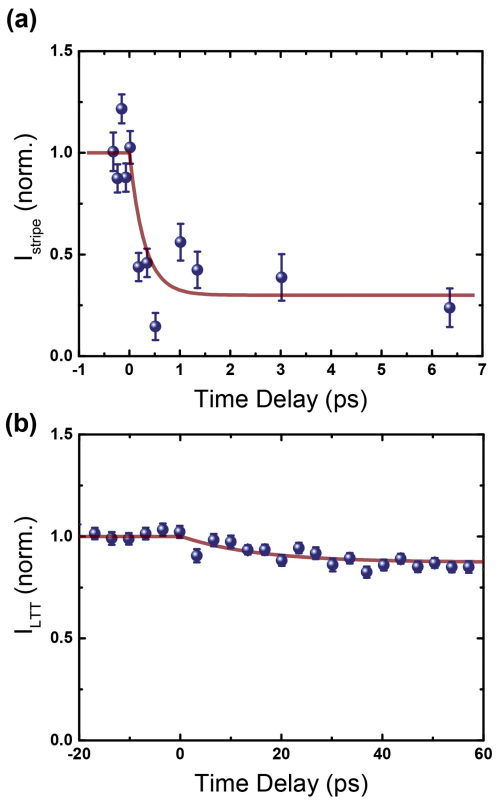

Fig. 8: (a) Transient intensity of the charge stripe order diffraction peak in $La_{1.875}Ba_{0.125}CuO_4$ measured at the (0.24 0 0.5) wave vector. Mid-IR excitation, resonant with the in-plance Cu-O stretching mode, at 1.9 mJ/cm^2 fluence results in a prompt sub-picosecond decrease of the scattered intensity. The red solid line represents an exponential function with a time constant set to 300 fs, i.e. the resolution of the experiment. (b) Light-induced changes in the intensity of the (001) diffraction peak (reflecting the LTT distortion) in the same $La_{1.875}Ba_{0.125}CuO_4$ crystal under same excitation conditions. The red solid is a single exponential fit to the data yielding a time constant of 15 ps. Figures adapted from Ref. 45.

48 Fink J.; Soltwisch V.; Geck J.; Schierle E.; Weschke E.; Büchner B. Phase diagram of charge order in $La_{1.8-x}Eu_{0.2}Sr_xCuO_4$ from resonant soft x-ray diffraction. Phys. Rev. B 2011, 83, 092503.
49 Dmitrienko V. Forbidden reflections due to anisotropic x-ray susceptibility of crystals. Acta Crystallographica Section A: Crystal Physics, Diffraction, Theoretical and General Crystallography 1983, 39, 29.

The time-resolved resonant soft X-ray diffraction experiments were performed on a $LBCO_{1/8}$ single crystal, held at base temperature T = 13 K in the stripe-ordered, LTT-distorted phase. Mid-infrared 200 fs pulses, tuned to the 85 meV (14.5 μm wavelength) resonance of the infrared-active in-plane Cu-O stretching vibration[50], were used for excitation. The excitation fluence was kept at 1.9 mJ/cm^2, comparable to the conditions of the light-induced superconductivity transition studied in $LESCO_{1/8}$[36].

The time-dependent integrated scattering intensity of the (0.24 0 0.5) stripe order diffraction peak in response to the mid-infared excitation is shown in Figure 8(a) above, showing a prompt decrease by about 70%. These results showed that the mid-infrared pulses melt the stripe order on a sub-picosecond timescale, implying that the ultrafast formation of the superconducting state and the melting of charge modulations are intimately connected.

In contrast, the evolution of the LTT phase, as probed by the (001) diffraction peak, was very different from that of the stripe order. The integrated scattered intensity of this structural peak dropped by only 12%, and with a much longer time constant of 15 ps (see fitted red solid line), which is likely determined by acoustic propagation when considering that the relaxation of the LTT distortion requires the lattice planes to expand.

3.2 Light-induced superconductivity and nonlinear lattice dynamics in $YBa_2Cu_3O_{6+x}$

A fascinating new effect induced by resonant lattice excitation was recently discovered in the bilayer high-temperature superconductor $YBa_2Cu_3O_{6+x}$. Similar to the materials discussed above, the superconducting phase requires coherent tunneling between stacks of bilayers, which is lost above the transition temperature T_C. Resonant lattice excitation was shown to enhance this coupling below T_C, and to induce coherent interlayer transport at temperatures up to more than 300K, far above the equilibrium transition temperature [51, 52].

---

50 Homes C.C. ; Hücker M.; Li Q. ; Xu Z.J.; Wen J.S.; Gu G.D.; Tranquada J.M. ; Determination of the optical properties of $La_{2-x}Ba_xCuO_4$ for several dopings, including the anomalous x=1/8 phase. Phys. Rev. B 2012, 85, 134510.

51 Hu W.; Kaiser S.; Nicoletti D.; Hunt C.R.; Gierz I.; Hoffmann M.C.; Le Tacon M.; Loew T.; Keimer B.; Cavalleri A.; Optically enhanced coherent transport in $YBa_2Cu_3O_{6.5}$ by ultrafast redistribution of interlayer coupling", Nature Mat. 2013, 13, 705.

52 Kaiser S.; Hunt C.R.; Nicoletti D.; Hu W.; Gierz I.; Liu H.Y.; Le Tacon M.; Loew T.; Haug D.; Keimer B.; Cavalleri A.; Optically induced coherent transport far above Tc in underdoped $YBa_2Cu_3O_{6+x}$. Phys. Rev. B 2014, 89, 184516.

$YBa_2Cu_3O_{6.5}$ (T_C = 50 K) crystallizes in an orthorhombic crystal structure and comprises bilayers of CuO_2 planes, separated by an insulating Yttrium layer as shown in Fig. 9(a). The interbilayer region is composed of Cu-O chains, which control the hole doping of the planes. A characteristic of the superconducting sate is the coherent interbilayer tunneling, which has a clear signature in the THz optical properties as shown in the upper panel of Fig. 9(b) for a $YBa_2Cu_3O_{6.6}$ sample. Above the transition temperature of 59 K, the reflectivity is featureless in the THz region, while a clear edge appears in the superconducting state[53]. This edge results from supercurrent oscillations between coupled bilayers and is called Josephson plasma resonance.

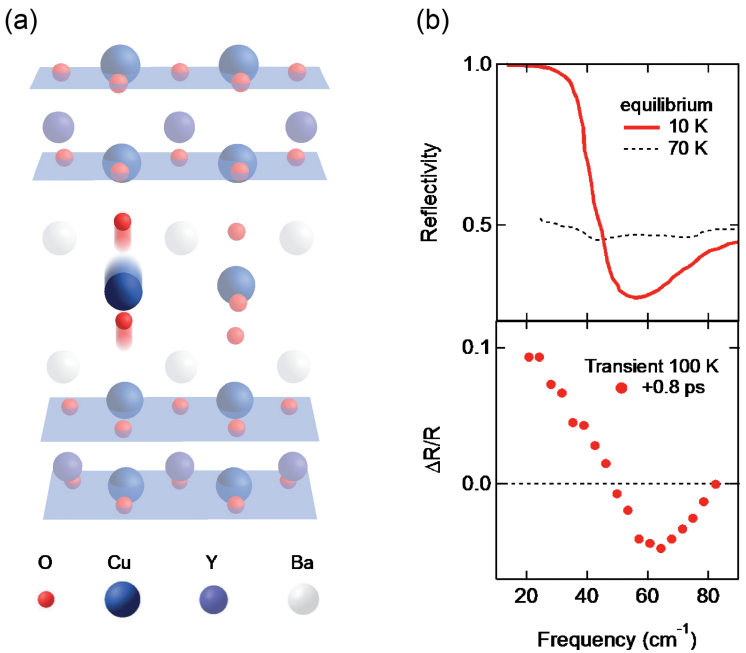

Fig. 9: (a) Crystal structure of orthorhombic $YBa_2Cu_3O_{6.5}$ and a sketch of the resonantly excited B_{1u}-symmetry infrared-active phonon mode, comprising c-axis motions of the apical oxygen atoms between bilayers. (b) Upper panel: c-axis static frequency resolved reflectivity of $YBa_2Cu_3O_{6.6}$ above and below the transition temperature of 59 K. Lower panel: Light-induced changes in the reflectivity of $YBa_2Cu_3O_{6.5}$ 0.8ps after excitation (red dots) with 300-fs pulses at 15 μm wavelength, polarized along the c-axis. The base temperature was 100K. Figures are adapted from Refs. [52, 53, 55].

53 Timusk T.; The mysterious pseudogap in high temperature superconductors: An infrared view. Solid State Commun. 2003, 127, 337.

The lower panel of Figure 9(b) shows the reflectivity changes of $YBa_2Cu_3O_{6.5}$ at 100 K base temperature, twice the transition temperature of 50 K, 0.8 ps after the excitation with 300 fs 15 μm mid-infrared pulses, resonant with the the B_{1u} symmetry phonon mode of Figure 9(a).

For these measurements, single-cycle THz pulses were generated by optical rectification in a nonlinear optical crystal, and their field measured after reflection from the sample by electro-optic sampling. Following resonant lattice excitation above T_C, the sample undergoes a transition in a non-equilibrium state with striking similarities to the equilibrium superconducting state, featuring a reflectivity edge that can be attributed to coherent interbilayer tunneling. Signatures of the Josephson plasma resonance have been found to follow resonant lattice excitation at temperatures up to 300 K in $YBa_2Cu_3O_{6.5}$.

In addition to the reflectivity edge at ~30cm^{-1}, which indicates interbilayer tunneling below T_C, the reflectivity of YBCO features a second edge at higher frequencies, a result of coherent transport between the neighboring CuO_2 planes of individual bilayers. While interlayer coherence only exists below T_C, signatures of intrabilayer coupling have been suggested to persist up to 150 K in $YBa_2Cu_3O_{6.5}$ [54]. In a series of experiments set out to explore the response of both junctions to resonant lattice excitation using broadband THz pulses, the appearance of interbilayer tunneling has been shown to come at the expense of intrabilayer coupling.

In search of a physical explanation of this highly exotic state, the underlying nonlinear lattice dynamics were investigated by femtosecond hard x-ray diffraction at the LCLS free electron laser.[55] As the direct product $B_{1u} \otimes B_{1u}$ is of A_g symmetry, the resonantly driven B_{1u} phonon mode of Figure 9(a) can only couple to Raman-active phonons of A_g symmetry as discussed in the introduction. Density Functional Theory (DFT) calculations identified four out of the eleven A_g Raman modes – all involving c-axis motions of the apical Oxygen and planar Copper atoms – to couple strongly to the driven B_{1u} lattice vibration. According to the theory of nonlinear phononics, the crystal lattice is expect to be promptly dis-

54 Dubroka A.; Rössle M.; Kim K. W.; Malik V. K.; Munzar D.; Basov D. N.; Schafgans A. A.; Moon S. J.; Lin C. T.; Haug D.; Hinkov V.; Keimer B.; Wolf T.; Storey J. G.; Tallon J. L.; Bernhard C.; Evidence of a precursor superconducting phase at temperatures as high as 180 K in $RBa_2Cu_3O_{7-\delta}$ (R=Y,Gd,Eu) superconducting crystals from infrared spectroscopy, Phys. Rev. Lett. 2011, 106, 047006

55 Mankowsky R.; Subedi A.; Först M.; Mariager S.O.; Chollet M., Lemke H.T.; Robinson J.S.; Glownia J.M.; Minitti M.P.; Frano A.; Fechner M.; Spaldin N.A.; Loew T.; Keimer B.; Georges A.; Cavalleri A.; Nonlinear lattice dynamics as a basis for enhanced superconductivity in $YBa_2Cu_3O_{6.5}$. Nature 2014, 516, 71.

placed into a new, transient structure along the linear combination of the atomic motions governed by these Raman modes.

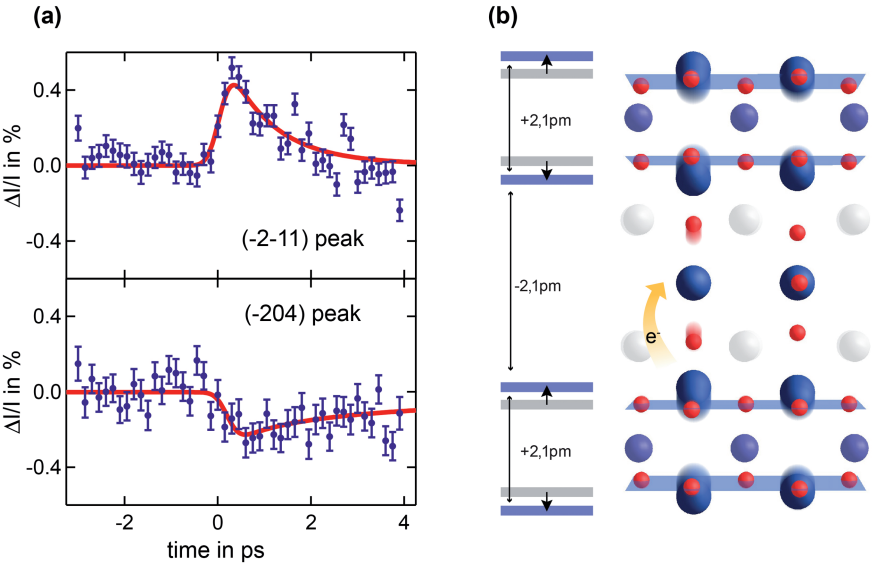

Fig. 10: (a) Relative changes in diffracted intensity of the (-2 -1 -1) and the (-2 0 4) Bragg peaks in $YBa_2Cu_3O_{6.5}$, following resonant excitation of the B_{1u}-symmetry mode measured at 100 K base temperature, above $T_c = 50$ K. Results of simultaneous fits to all data are shown as solid red lines (see text for details). (b) Sketch of the reconstructed transient crystal structure of $YBa_2Cu_3O_{6.5}$ at the peak signal. The atomic displacements from the equilibrium structure involve a decrease in interbilayer distance, accompanied by an increase in intrabilayer distance. Figures are adapted from Ref. 55.

Figure 10(a) shows the signature of the lattice dynamics following lattice excitation by 4 mJ/cm^2 mid-infrared pulses at 15 µm wavelength, the same excitation for which the enhancement of superconductivity was found, exemplary for the (-2-11) and (-204) diffraction peaks at 100 K sample temperature. The measurements were obtained using 50 fs x-ray pulses with 6.7 keV photon energy from the LCLS Free Electron Laser. A prompt change in diffracted intensity was observed, as expected from the rearrangement of the atoms in the unit cell predicted by the model of nonlinear phonics. The decay back to the equilibrium structure happens on the same timescale as the relaxation of the induced coherent interlayer transport measured previously, indicating an intimate connection[51, 52].

The exact sign and amplitude of the diffracted intensity changes carries information on the atomic motions the lattice rearrangement is comprised of. In order to reconstruct the transient crystal structure, the computed coupling

strengths to the respective A_g Raman modes were combined with structure factor calculations, predicting the changes in diffraction intensity of all measured Bragg peaks for a given B_{1u} amplitude. By using these results and the signal rise and decay times from the THz measurements, all measured Bragg peaks have been fitted simultaneously with only two fitting parameters, the amplitude of the resonantly driven infrared-active B_{1u} mode and the relative contribution of the two decay times found in the THz experiment (see Ref. 55 for details of this procedure). The resulting fits are shown as red lines in panel (a) of Figure 10.

The transient crystal structure as shown in panel (b) of the same Figure is composed of an increase in the in-plane O-Cu-O bond buckling and a decrease in apical Oxygen – planar Copper distance. Finally, the intrabilayer distance increases, whereas the CuO_2 planes of different bilayers move closer together, effectively enhancing the interbilayer coupling. This last observation is intuitively consistent with the broadband THz measurements, which indicate that the appearance of interbilayer coherence comes at the expense of intrabilayer coupling strength.

Density Functional Theory calculations using the transient crystal structure further predict a charge transfer from the CuO_2 planes to the Cu-O chains, effectively increasing the hole doping of the planes. Such self-doping has recently been found to accompany the temperature-driven equilibrium metal-superconductor transition and might emerge as key in explaining the formation of the superconducting phase[56]. Further experiments will show, whether the charge redistribution predicted here is comparable in magnitude.

Finally, a recent theoretical study investigated the effect of the lattice dynamics presented here on superconductivity and charge order. Their results predict an increase in the transition temperature T_C by up to 100% and a suppression of charge order[57]. The latter was investigated recently in a resonant soft x-ray diffraction study, during which a partial melting of charge order was indeed observed, consistent with the theoretical results[58].

---

56 Magnuson M.; Schmitt T.; Strocov V.N.; Schlappa J.; Kalabukhov A. S.; Duda L. C.; Self-doping processes between planes and chains in the metal-to-superconductor transition of YBa2Cu3O6.9. Sci. Rep. 2014, 4, 7017.

57 Raines Z.M.; Stanev V.; Galitski V.M.; Enhancement of superconductivity via periodic modulation in a three-dimensional model of cuprates. Phys. Rev. B 2015, 91, 184506

58 Först M.; Frano A.; Kaiser S.; Mankowsky R.; Hunt C.R.; Turner J.J.; Dakovski G.L.; Minitti M.P.; Robinson J.; Loew T.; Le Tacon M.; Keimer B.; Hill J.P.; Cavalleri A.; Dhesi S.S.; Femtosecond x rays link melting of charge-density wave correlations and light-enhanced coherent transport in $YBa_2Cu_3O_{6.6}$. Phys. Rev. B 2014, 90, 184514

4 Conclusions

We have shown how intense light fields at mid-infrared wavelengths can be used to drive condensed matter into transient structures that are not achievable at equilibrium. The coupling between different vibrational modes is key to this effect, which was demonstrated for third-order anharmonic coupling. In complex oxides, prototypical examples of correlated electron materials, these lattice distortions can lead to electronic and magnetic phase changes, including insulator-metal transitions and even enhanced superconductivity. In the spirit of static materials engineering in complex oxide heterostructures, light-induced deformations of the crystal lattice can also be used to achieve functional control across hetero-interfaces dynamically. These phenomena are highly interesting and open up new ways to control the crystal lattice and the functionality of materials, and may open up new strategies for materials discovery and lead the synthesis of condensed matter with improved functionality.